RSC Advances

PAPER

View Article Online
View Journal | View Issue



Cite this: *RSC Adv.*, 2024, **14**, 18750

# High-density polyethylene composites filled with micro- and nano-particles of nickel ferrite: magnetic, mechanical, and thermal properties†

Sarah Baayyad,[a] Youssef Esshouba,[a] Soufiane Barhoumi,[a] El Kébir Hlil,[c] Siham Ez-Zahraoui,[a] Fatima-Zahra Semlali,[a] Tarik Mahfoud,[b] Hassan El Moussaoui*[b] and Mounir El Achaby*[a]

With the increasing demand of new magnetic materials for modern technological application alternatives to conventional magnetic materials, the development of lightweight polymer magnetic composites has become a prominent research area. For this perspective, a new magnetic material was developed using 30 wt% nickel ferrite micro and nanoparticles as fillers for a high-density polyethylene matrix. The development process began with the synthesis of NF-micro and NF-nanoparticles using solid-state and co-precipitation techniques, respectively, followed by extrusion molding and injection molding. The success of the synthesis process and the purity of the spinel structure phase were confirmed. Additionally, using the extrusion process produced polymer magnetic composite materials with a good distribution of magnetic particles within the polymer matrix, resulting in good magnetic properties and enhanced mechanical properties of the polymer magnetic materials.

Received 8th April 2024
Accepted 3rd June 2024

DOI: 10.1039/d4ra02643h

rsc.li/rsc-advances



## 1. Introduction

The development of magnetic materials for modern technology applications has become a prominent research area due to the rapid growth of electronic devices in different fields.[1] In particular, spinel ferrite materials, with their good magnetic, structural, optical, and electrical properties, make them desirable for several applications.[2,3] Generally, spinel ferrites are a group of mixed oxides that have a characteristic general formula $MFe_2O_4$, in which M can be Fe Co, Ni, Zn, Mn, or other metal cations.[4,5] The unit cell of spinel ferrite is face centered cubic (fcc).[6] Spinel ferrite can be divided into three groups depending on its crystal structure, normal, inverse, and mixed inverse spinel.[7] Normal spinel is created when tetrahedral sites are occupied by $M^{2+}$ and octahedral sites are occupied by $Fe^{3+}$. On the other hand, when tetrahedral sites are occupied by $Fe^{3+}$and octahedral sites are shared by an equal amount of $Fe^{3+}$ with $M^{2+}$, an inverse spinel structure is formed.[8] In the case of mixed ferrites, the cations occupy both tetrahedral sites and octahedral sites, represented by a general formula can be written as $(M_{1-\delta}{}^{2+}Fe_{\delta}^{3+})[M_{\delta}{}^{2+}Fe_{2-\delta}{}^{3+}]O_4$ where $\delta$ is called the degree of inversion.[9] Among the spinel ferrites, nickel ferrite ($NiFe_2O_4$) is an inverted spinel magnetic ferrite material with $Fe^{3+}$ ions distributed equally at octahedral and tetrahedral sites and $Ni^{2+}$ ions only at octahedral sites.[10,11] Due to their high resistivity, low coercivity, moderate saturation magnetization and low hysteresis losses, nickel ferrites are categorized in the class of soft ferrites. These soft magnetic materials also offer other favorable properties, such as high permeability at high frequency, mechanical hardness, and electrochemical stability. Due to these features, these ferrites are successfully utilized in a wide range of applications.[12,13] Several techniques are used for the synthesis of $NiFe_2O_4$, such as hydrothermal,[14–17] sol–gel,[18–20] and sonochemical,[21,22] co-precipitation is also used to produce nickel ferrite nanoparticles.[23,24]. The ceramic method is still the most common and widely used technique for the production of nickel ferrite particles, by mixing the oxidized raw materials and sintering at high temperature.[25] Soft magnetic ferrites, in general, and,nickel ferrite, in particular, possess useful properties such as a significant saturation magnetization, a high electrical resistivity, low electrical losses, thus making them an attractive class of magnetic materials suitable for a large number of applications.[26] Despite their valuable properties, soft magnetic materials have limitations. They can be brittle, making them susceptible to damage from mechanical stress and impacts, which restricts their use in applications needing high durability. Their fabrication and processing are energy-intensive and costly, often requiring high temperatures.

[a]*Materials Science, Energy and Nanoengineering Department (MSN), Mohammed VI Polytechnic University (UM6P), Lot 660 – Hay Moulay Rachid, Ben Guerir, 43150, Morocco. E-mail: mounir.elachaby@um6p.mamailto*

[b]*Moroccan Foundation for Advanced Science, Innovation and Research (MAScIR), Rabat Design Center, Rue Mohamed El Jazouli, Madinat El Irfane, 10100 Rabat, Morocco. E-mail: h.elmoussaoui@mascir.ma*

[c]*Institut Néel, CNRS et, Université Joseph Fourier, BP 166, F-38042 Grenoble Cedex 9, France*

† Electronic supplementary information (ESI) available. See DOI: https://doi.org/10.1039/d4ra02643h

Additionally, they are dense and heavy, which is a disadvantage in weight-sensitive applications.[27,28] For these reasons, modern research focuses on developing new materials with low energy consumption and excellent properties. These materials, which are also lightweight, are particularly beneficial in applications such as aerospace, automotive, and consumer electronics, where weight reduction is critical. Additionally, properties of polymer composites can be customized by varying the type and amount of magnetic particles and the choice of polymer matrix, leading to an optimal balance of magnetic, mechanical, and thermal properties.[28] Polymer composite materials are a combination of two materials, a matrix polymer whose role is to hold the reinforcement materials, and reinforcement materials, which transmit the loads to the matrix. Therefore, they define most of the mechanical characteristics of the material, such as resistance and rigidity, as well as the magnetic, optical, and electrical properties of the final composite materials.[29,30] Many researchers have attempted to synthesize polymer magnetic composite materials. Direct mixing of the magnetic particles with the polymer is the most conventional and easiest way of preparing magnetic polymer composite materials. Melt blending and grand solution blending are commonly employed techniques for achieving this combination.[31] Wilson JL, *et al.*[32] have synthesized polymer magnetic composite materials of poly(methylmethacrylate) doped with varying concentrations of iron nanoparticles for electromagnetic device application. I. Kong, *et al.* used $Fe_3O_4$ as a filler in matrix reinforced thermoplastic nature rubber (TPNR) to form polymer magnetic composite materials using melt blending methods.[33] The same technique has been used by Chung, *et al.* to produce a flexible cross-linked shape memory polyurethane filled with ferromagnetic particles of $Fe_3O_4$.[34] Other techniques for the creation of magnetic polymer composite materials include methods such as the suspension polymerization process used by Robson T. Araujo, *et al.* to Synthesize of Poly(vinyl pivalate)-Based magnetic nanocomposites with $Fe_2O_4$ as a reinforcing material for medical application.[35] In recent years, composite materials based on thermoplastic polymer matrix have attracted researcher's attention. Thermoplastic matrices are composed of linear chains, which can be transformed in the molten state. In various manufacturing processes, these thermoplastic matrices are heated, then subjected to molding, injection, extrusion, or thermoforming, and subsequently cooled. This ensures that the final product maintains its intended shape. This operation is reversible, enabling the thermoplastic matrices to be in different forms. Moreover, they exhibit non-oxidizing properties, high corrosion resistance, and serve as excellent thermal and electrical insulators. Owing to their lightweight nature, high mechanical strength, and resilience against environmental factors, thermoplastics emerge as ideal materials for numerous applications.[36] All these characteristics make them a good choice for matrix materials in magnetic polymer composite materials.

To the best of our knowledge, polymer magnetic composite materials soft magnetic behavior produced by curing mixtures of $Fe_3O_4$ magnetic particles and elastomeric matrices have been proposed. Therefore, this study introduces new magnetic composite materials using high density polyethylene (HDPE) as a matrix and $NiFe_2O_4$ microparticles and nanoparticles as fillers, utilizing extruding molding. The main objective is to investigate the effect of $NiFe_2O_4$ magnetic particles on HDPE and their impact on its magnetic and mechanical properties. Additionally, a comparative study examines the effect of nanoparticles and microparticles on HDPE matrix.

## 2. Materials and methods

### 2.1. Materials

Chemicals with high purity were purchased from Sigma-Aldrich and used without further purification. In the solid-state reaction Nickel oxide (NiO) and Iron(III) oxide ($Fe_2O_3$) served as starting materials. In the Co-precipitation method, Nickel chloride hexahydrate ($NiCl_2 \cdot 6H_2O$) and ferric chloride hexahydrate ($FeCl_3 \cdot 6H_2O$) were used as precursor materials, polyethylene high density (HDPE) was used as the polymer matrix in order to prepare the composite material.

### 2.2. Synthesis of $NiFe_2O_4$ nanoparticles with co-precipitation reaction

The Co-precipitation technique was employed to prepare NF-nano particles. Firstly, 2.5 g of 0.21 M of $CoCl_2 \cdot 6H_2O$ and 5.7 g of 0.41 M of $FeCl_3 \cdot 6H_2O$ were dissolved in 50 ml of distilled water separately using magnetic steering at room temperature for 30 min. Thereafter, the two solutions were blended into one solution and kept under magnetic steering. The pH of the solution was adjusted to 11 by the addition of 3 M NaOH. The solution was kept at a temperature of 80 °C for 60 min using magnetic steering. At the end of the synthesis, a small amount of oleic acid was added to the solution as a surfactant to minimize the agglomeration of the nanoparticles. The resulting precipitate was washed using a centrifuge to remove any sodium and chlorine compounds. The precipitate was then dried at 100 °C overnight, and the resulting powder was finally calcined at 400 °C for 2 hours. Fig. 1a illustrates the synthesis steps.

### 2.3. Synthesis of $NiFe_2O_4$ microparticles with solid state reaction

As illustrated in Fig. 1b, to synthesize NF-micro particles using a solid-state reaction, the precursors were ground in stoichiometric amounts in an agate mortar for about 1 hour at room temperature to get a homogenous mixture, then calcined at 1200 °C for 6 h in air. The prepared powder was then combined with acetone and 532.5 mm stainless steel balls before being sealed in a 250 ml stainless steel bottle. A Fritsch 6 pulverisette was used for mechanochemical milling for 2 hours at 250 rpm with a ball-to-powder mass ratio of 20 : 1.

### 2.4. Composite preparation

To prepare magnetic composite material with a polymeric matrix, 30% of each powder, previously synthesized through solid-state and co-precipitation methods, was blended with 70% HDPE separately as showed in Fig. 1c. This blending

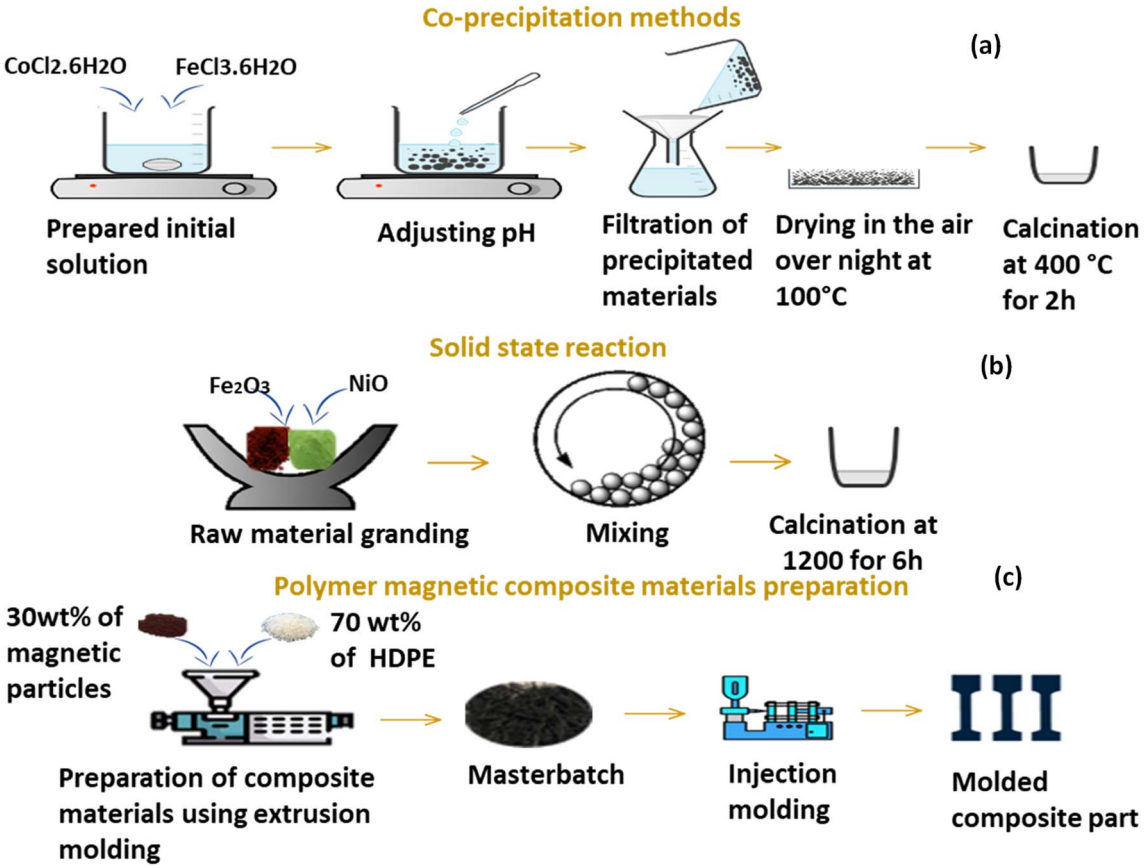


Fig. 1 Schematization of (a) co-precipitation method, (b) solid state route and fabrication of composite materials.

process was conducted using a Thermos Scientific Process twin screw co-rotating extruder with a screw speed of 70 rpm. The temperature profile was ranged from 170 °C to 190 °C. The resulting melts were then cooled and quenched in a water bath, followed by manual pelletization using scissors into granules measuring of 2–3 mm in length. The composite materials were molded using Micro-Presse injection Babyplast 6/12 Standard-Chronoplast, the temperature setting for the injection press barrel and the nozzle were 175 °C and 180 °C, respectively, the mold was maintained at room temperature, and the cooling time was set to 6 s.

## 3. Characterization techniques

### 3.1. X-ray diffraction (XRD)

The X-ray diffraction (XRD) analysis of the ferrite particles was conducted using a D8-Discover diffractometer, BRUKER (Nanotechnology Platform, MSN Laboratory). The CuK radiation ($\lambda = 1.5418°$) is used to scan the samples in the range of 5–80° with a step size of 0.01°, while the voltage and current are set at 45 kV and 100 mA, respectively.

### 3.2. Fourier transform infrared spectroscopy (FTIR)

Fourier-transform infrared spectra of the synthesized powder neat HDPE, and composite materials were recorded using a FTIR, PerkinElmer Spectrum 2000 equipped with an ATR accessory. Each spectrum was obtained in 600–4000 $cm^{-1}$ range, with an accumulation of 16 scans and a resolution of 4 $cm^{-1}$.

### 3.3. Raman spectroscopy

A Witec alpha-300RA apparatus with a 532 nm Nd:YAG laser was used for the Raman investigations. Raman spectra were acquired using an 1800 g $mm^{-1}$ grating and a 0.95 numerical aperture objective with a laser excitation intensity of 3 mW.

### 3.4. Scanning electronmicroscopy

The morphological properties of magnetic particles as well as neat HDPE and HDPE/$NiFe_2O_4$ are investigated using a Zeiss EVO 10 scanning electron microscope (Carl Zeiss Microscopy, GmbH, Jena, Germany).

### 3.5. UV-vis spectroscopy

UV-visible absorption spectra were acquired using a PERSEE T8DCS within the wavelength range of 200–800 nm. This analysis was conducted to investigate the optical properties of both the particles and the composite materials, and to study the interactions between the polymers and the reinforcing particles.

### 3.6. Vibrating sample magnetometer

Our study leverages a high-resolution Vibrating Sample Magnetometer (VSM) with a remarkable $10^{-11}$ $Am^2$ resolution.

The instrument's magnetic field control spans ±7 T, facilitating precise measurements, while its temperature range of 1.8 to 400 K allows for a comprehensive exploration of magnetic properties across varying thermal conditions.

### 3.7. Thermogravimetric analyses (TGA)

The thermal properties of the composites were determined using Discovery TGA (TA Instruments) over a temperature range from room temperature to 700 °C under air, with a heating rate of 10 °C $min^{-1}$.

### 3.8. Differential scanning calorimetry (DSC)

DSC analysis of HDPE and polymeric composites was performed using TA instruments (Discovery DSC) to determine melting temperatures and study the thermal properties of the composite materials.

## 4. Results and discussions

### 4.1. Characterization of the as-synthesized magnetic particles

**4.1.1. Structural characterization.** X-ray results shown in Fig. 2, the apparent of principal peaks (111), (220), (311), (222), (400), (422), (511) and (440) indexed by standard JCPDS (00-044-1485) confirm that the diffraction patterns of the synthesized particles are in a good match with the cubic spinal structure of $NiFe_2O_4$. Additionally, no peaks corresponding to impure phases are detected. A small noise was recorded in the XRD patterns of NF-nano due to the amorphous nature of the oleic acid used in the synthesis.[37] Crystallite size was calculated by Scherrer approach size eqn (2) by taking the strongest peak of XRD pattern. The lattice parameter ($a$) is calculated using eqn (1) where ($hkl$) is the Miller index and ($d$) is the measured interplanar spacing. The volume of the unit cell for the cubic system has been calculated using eqn (3), with $a_{exp}$ is the lattice parameter.

$$a = d(h^2 + k^2 + l^2)^{1/2} \quad (1)$$

Table 1 Lattice parameter, volume of cell and crystallite size

| Samples | Lattice parameter (Å) | Volume of cell ($Å^3$) | Crystallite size (nm) |
|---|---|---|---|
| NF-micro | 8.340 | 580.090 | 139.080 |
| NF-nano | 8.378 | 588.050 | 26 |

$$d = \frac{0.94\lambda}{\beta \cos \theta} \quad (2)$$

$$V = a_{ext}{}^3 \quad (3)$$

Lattice parameters and average crystallite size of the samples are presented in Table 1, which shows that the crystallite size calculated using eqn (2) by taking the most intense peak (311) was found to be around 26 nm for nanoparticles and 139.08 nm for microparticles. The results also indicate that there is a difference between the values of the lattice parameters of microparticles and nanoparticles, as we can notice that the lattice parameters increase with the decrease in particle size.

Raman spectroscopy is used to investigate the physical properties of $NiFe_2O_4$ particles due to the strong correlation between the crystal structure and the lattice vibration.[38] The Raman spectra of NF-nano and NF-micro particles are shown in Fig. 3. This figure shows that the $NiFe_2O_4$ particles have five major bands. $A_{1g}$ (682–683 $cm^{-1}$), $E_g$ (320–322 $cm^{-1}$) and 3 $T_{2g}$ (552–556 $cm^{-1}$, 453–475 $cm^{-1}$, and 200–203 $cm^{-1}$).[39] The $A_{1g}$ mode corresponds to symmetric stretching of oxygen atoms along Fe–O and Ni–O bonds in the tetrahedral site. $E_g$ mode is related to symmetric bending of oxygen with respect to the metal ion, $T_{2g}(3)$ corresponds to asymmetric bending of oxygen,$T_{2g}(2)$ corresponds to asymmetric stretching of Fe (Ni) and O in the octahedral site, $T_{2g}(1)$ is due to translational movement of the tetrahedron (metal ion at tetrahedral site together with four oxygen atoms).[40] Additionally, the figure also

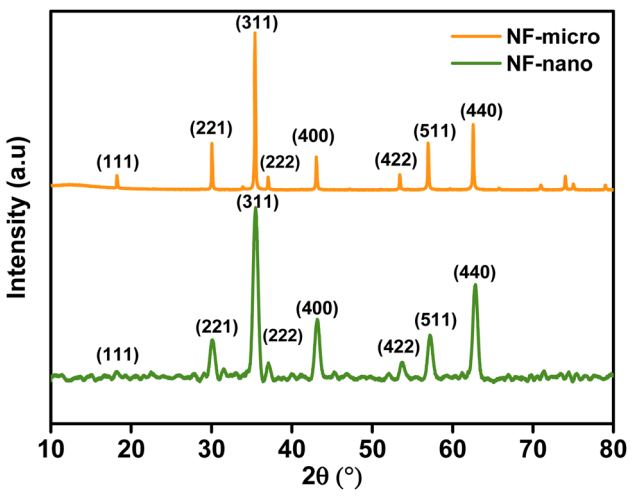


Fig. 2 XRD pattern of NF-micro and NF-nano powder.

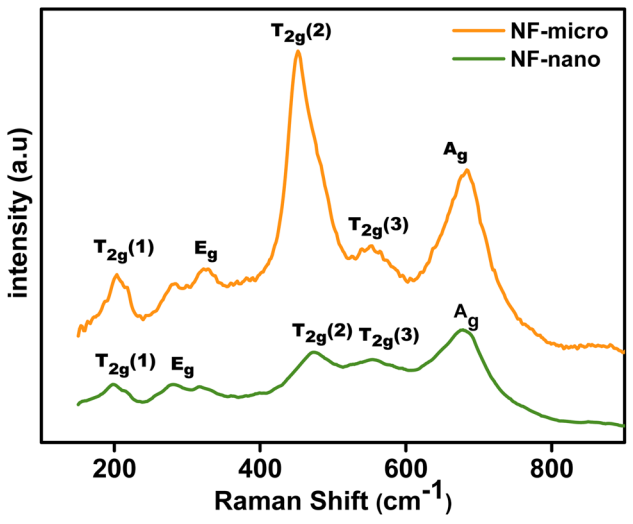


Fig. 3 Raman spectra of NF-micro and NF-nano.

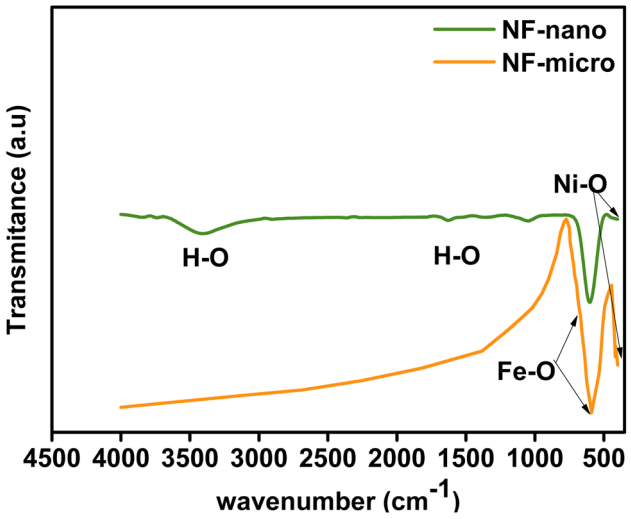


Fig. 4 FTIR spectra of NF-micro and NF-nano.

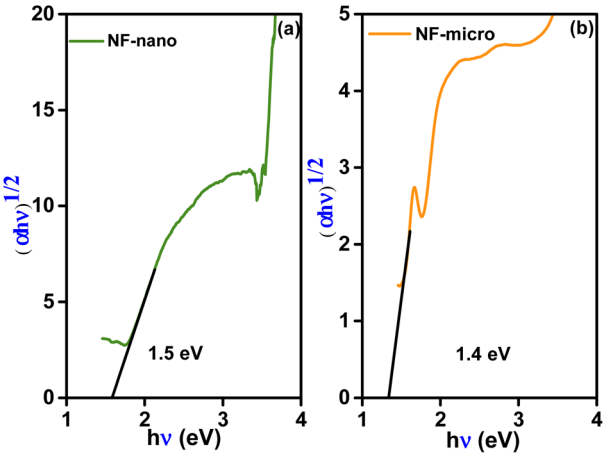


Fig. 5 (a) Plots $(\alpha h\upsilon)^{1/2}$ *vs.* (b) photon energy ($h\nu$) for microparticles and nanoparticles.

show that the Raman mode shifted to a higher frequency and the Raman peaks became narrower in the case of NF-micro, due to cation redistribution and increases in crystallinity with the annealing temperature.[41,42].

FTIR spectra of NF-nano and NF-micro particles are presented in Fig. 4 in the range of 500–600 $cm^{-1}$ at room temperature. According to the literature,[43,44] the two FTIR absorption bands are identified between 500 and 600 $cm^{-1}$ and between 300 and 400 $cm^{-1}$ respectively. These bands are attributed to the metal–oxygen stretching vibrations in the tetrahedral and octahedral sites, corresponding to the characteristic of ferrite. Moreover, additional vibrational bands associated with the H–*O*–H bond were also observed at 3400 $cm^{-1}$, 2927 $cm^{-1}$ and 1623 $cm^{-1}$, signifying the stretching of absorbed water molecules in the case of NF-nano particles synthesized using the co-precipitation route.[45,46]

UV-visible spectroscopy proves to be a valuable method for providing significant insights into the impact of crystallite size on the band gap energy ($E_g$) of spinel $NiFe_2O_4$. Fig. S1† shows the UV-visible reflectance spectra of NF-nano and NF-micro particles, recorded in the range of 200–800 nm. The spectrum indicate that nickel ferrite exhibits a weak reflectance intensity in both the UV and visible regions, aligning with findings reported in several works in the literature.[47,48] The optical band gap of NF-micro and NF-nano particles is calculated using the Kubelka–Munk function of reflectance $F(R)$ eqn (4) as shown in Fig. 5.

$$F(R) = \frac{(1-R)^2}{2R} \quad (4)$$

The absorption coefficient ($\alpha$) is directly proportional to the Kubelka–Munk function $F(R)$ and the equation used to determine the band gap of both particles.[49]

$$(\alpha h\nu)^n = A(h\nu - E_g) \quad (5)$$

where $A$ is a constant relative to the material, $h\nu$ the energy of a photon, the value of $n$ depends on the type of transition. $n = 2$ for direct transition and $n = 1/2$ for indirect transition, $n = 2/3$ for direct forbidden, and $n = 1/3$ for indirect forbidden.[50] The optical gap values for NF-micro and NF-nanoparticles were determined to be 1.4 eV and 1.5 eV, respectively. This value was found by plotting $(\alpha h\nu)^{1/2}$ *vs.* $h\nu$, where the optical band gaps ($E_g$) are the intercepts with the energy axes as shown in Fig. 5a and b. Notably, it's observed that the optical band gap of NF-micro particles is marginally smaller than that of NF-nano particles, suggesting a decrease in the band gap with an increase in particle size. This decrease in the band gap could be attributed to the basis of weak quantum confinement effects.[51]

**4.1.2. Morphological characterization.** The SEM images of NF-micro and NF-nano are indicated in Fig. 6. In the case of NF-micro particles synthesized through solid-state reaction, an uneven distribution of morphology and particle size is evident. Additionally, agglomeration within the sample is observed, attributed to the magnetic characteristics of the particles. Conversely, the figure illustrates that nanoparticles of $NiFe_2O_4$ prepared *via* the co-precipitation route exhibit a homogeneous distribution of particles and a pronounced formation of ferrite clusters. This behavior is attributed to the magnetic properties of the particles and the combination of primary particles held together by strong external interactions, such as van der Waals forces.[52]

**4.1.3. Magnetic characterization.** The magnetic properties of NF-micro and NF-nano particles, synthesized through solid-state reaction and co-precipitation methods, respectively, where investigated using a vibration sample magnetometer (VSM). Fig. 7 shows the representative M (H) curves for both types of particles, measured at room temperature. The curve shows that all samples exhibit soft magnetic properties with distinct hysteresis curves. The saturation magnetization, remanence magnitude, and coercivity field for both NF-nano and NF-micro particles are mentioned in Table 2. The value of saturation magnetization is increased from 18.16 (emu $g^{-1}$) for NF-nanoparticle to 49.94 (emu $g^{-1}$) for NF-micro particles, while

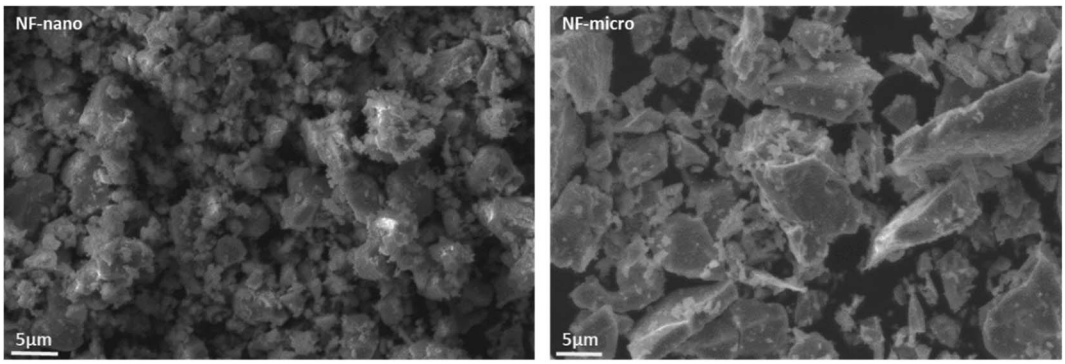


Fig. 6 SEM image of NF-nano and NF-micro.

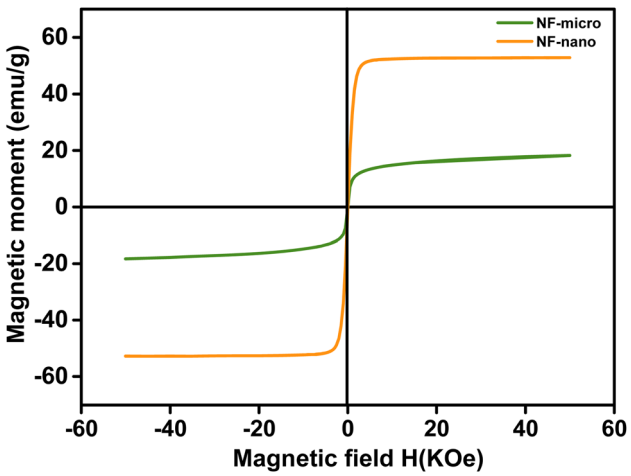


Fig. 7 Magnetic properties of $NiFe_2O_4$ nano and micro particles.

the value of coercivity is decreased from 0.022 (Koe) for NF-nano to 0.016 (Koe) for NF-micro. This results is related to the particles size, as the grain size increase, the saturation magnetization increases and the coercivity decreases.[53] The reduction in saturation magnetization (Ms) observed with smaller particle sizes in attributed to significant surface effects in these nanoparticles. In nanoparticles, the surface to volume ratio is so high that surface properties dominate the overall characteristics. The nanoparticle surface is thought to consist of canted or disordered spins that hinder the alignment of core spins along the external magnetic field direction, leading to a decrease in the saturation magnetization.[54] As particle size increases, it supports the formation of domain walls. This causes magnetization reversal to happen through domain wall motion, resulting in lower coercivity. Therefore, as particle size increases, the coercivity decreases.[55] Fig. S2a† shows the M(T) curve of $NiFe_2O_4$ ferrite nanoparticles. A significant drop in magnetization with increasing temperature indicates a sharp transition from ferromagnetic to paramagnetic. The Curie temperature ($T_c$), determined from the peak of dM(T)/dT, is measured at 840.19 k, which is slightly lower than 846.77 k observed for $NiFe_2O_4$ microparticles shown in Fig. 2. This difference can be attributed to the finite size-scaling effect.[56,57]

### 4.2. Characterization of composite materials

**4.2.1. Structural characterization.** The FTIR spectroscopy is used to investigate changes in chemical composition of neat HDPE, NF-nano/HDPE, and NF-micro/HDPE, and the results are shown in Fig. 8. The FTIR spectrum of neat HDPE shows the presence of two bands at 2915 $cm^{-1}$ and 2819 $cm^{-1}$, which correspond to asymmetric and symmetric stretching vibrations of single bond $CH_2$ single bond groups, respectively. At 1460 $cm^{-1}$, there is a C–H bending band of $CH_2$ groups. As well as at 720 $cm^{-1}$.[58] All the observed peaks are present in both pure HDPE and the composite materials. Notably, there are no additional peaks are formed, and there is no shift in the position of the peaks when compared to neat HDPE. This observation confirms the absence of any chemical interactions between the matrix and the fillers, reaffirming the integrity of the composite structure.[59]

Raman spectra of HDPE, NF-micro/HDPE, and NF-nano/HDPE are shown in Fig. S3.† The Raman Peaks of HDPE are found at 2882.25 $cm^{-1}$,2842.64 $cm^{-1}$, 2720.23 $cm^{-1}$, 1461.9 $cm^{-1}$, 1438.14 $cm^{-1}$, 1416.11 $cm^{-1}$, 1435.28 $cm^{-1}$, 1299.58 $cm^{-1}$, 1171.14 $cm^{-1}$, 1123.30 $cm^{-1}$, and 1062.87 $cm^{-1}$ as shown in Fig. S3a†.[60] The peaks in the range between 200 $cm^{-1}$-800 $cm^{-1}$ correspond to five active Raman modes of nickel ferrite particles, as shown in Fig. S3b.† According to these results, we can conclude that both NF-micro/HDPE and NF-nano/HDPE composite materials have been successfully

Table 2 Magnetic properties of $NiFe_2O_4$ micro and nanoparticles

| Sample | Grain size (μm) | $M_s$ (emu $g^{-1}$) | $M_r$ (emu $g^{-1}$) | $H_c$ (Koe) | $R$ | $T_c$ (K) |
|---|---|---|---|---|---|---|
| NF-micro | 20.180 | 49.940 | 1.50 | 0.016 | 0.012 | 846.77 |
| NF-nano | 0.005 | 18.160 | 0.30 | 0.022 | 0.170 | 840.19 |

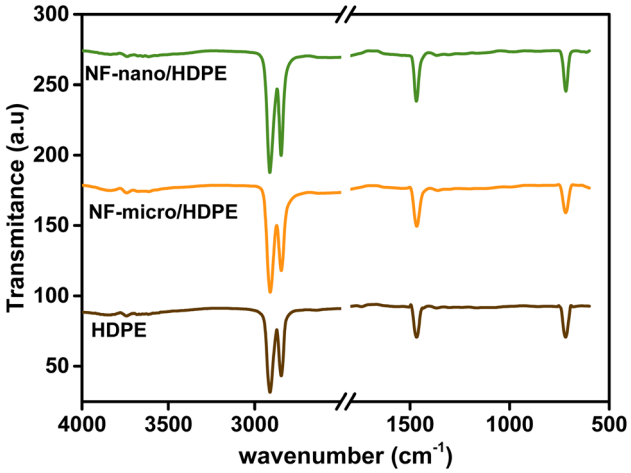


Fig. 8 FTIR spectra of HDPE polymer, NF-micro/HDPE and NF-nano/HDPE composites.

prepared, and which confirms FTIR results. The addition of ferrite particles to the HDPE matrix decreases the intensity of the Raman peaks and affects the crystallinity of the materials due to the incorporation of the particles into the HDPE matrix.

The optical characteristics of neat HDPE and composite materials, as well as their gap energy, were investigated using UV-visible spectroscopy. The UV-visible spectra of neat HDPE, NF-micro/HDPE, and NF-nano/HDPE are shown in Fig. S4.† A large reflectance band of HDPE in the visible light rang can be seen in the figure. Moreover, it's notable that both neat HDPE and the composite materials have a similar reflectance behavior, with a significance lower reflectance in composite materials due to the effect of magnetic particles on the reflectance of polymeric matrix. To estimate the gap energy of the composite materials, the Kubelka–Munk equation was used as well as all the equations mentioned before in the study of the UV-visible spectroscopy for magnetic particles, and the results are shown in Fig. S5.† it's can obviously notice from the figure that the value of the optical band gap decreases with the addition of magnetic particles to the polymeric matrix, which is connected in decrease of the reflectance intensity of composite materials and explained by the change in polymer structure.[61]

**4.2.2. Morphological characteristics.** The SEM-EDX images of the cross section of neat HDPE, NF-micro/HDPE, and NF-nano/HDPE composites shown in Fig. 9 were evaluated to visualize the degree of filler dispersion within the polymer matrix. The SEM image of neat HDPE shows a relatively smooth fractured surface in association with terraced markings, indicating weak resistance to crack propagation.[62] In the case of the NF-micro/HDPE composite, it is very clear that there is good dispersion of filler in HDPE, the NF-micro particles were uniformly distributed throughout the matrix, with minimal agglomerates as shown in the figure. In most of the micrographs, the added fillers can be seen as small white spots. For the NF-nano/HDPE composite materials, we can notice that there is no clear vision of the nanoparticles in the polymeric matrix, and the cross-section surfaces of NF-nano/HDPE and pure HDPE are

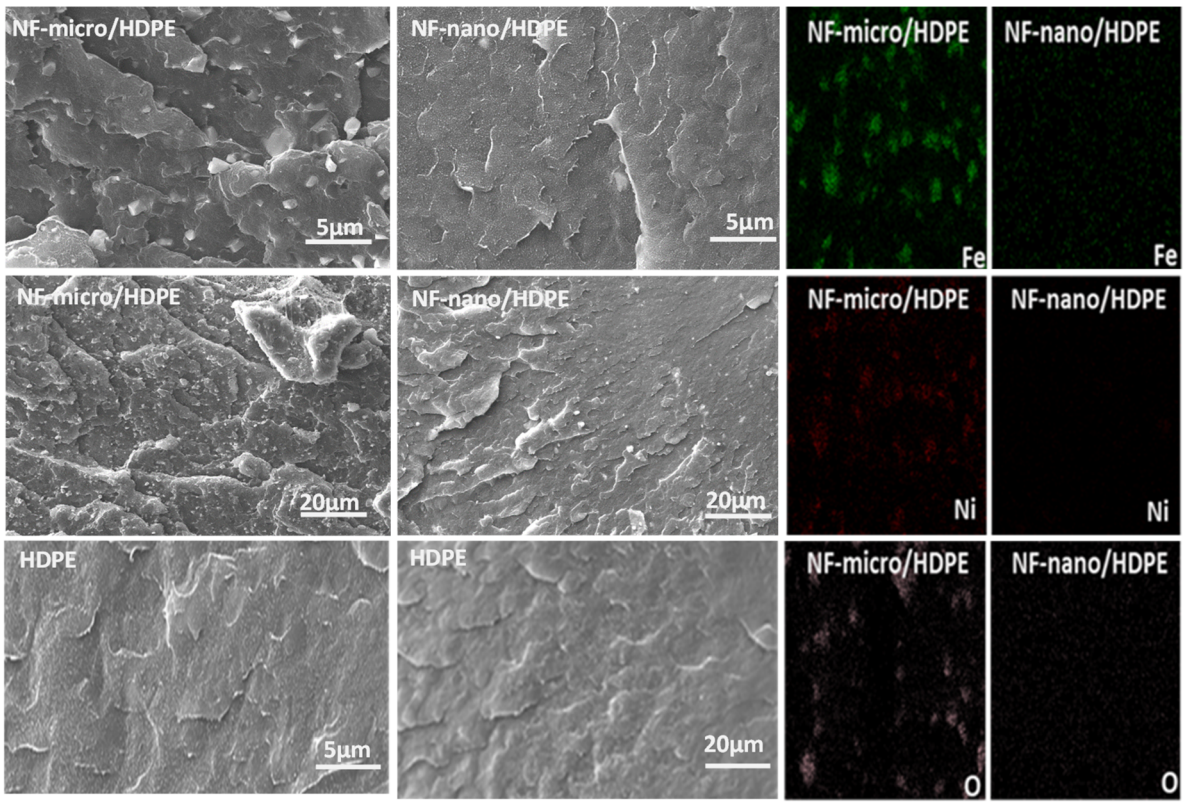


Fig. 9 Cross section SEM-EDX micrographs of the elaborated composites.

similar, which shows that the surface of the composite material has not undergone any type of treatment or modification. Overall, both NF-micro and NF-nano particles serve effectively as composite fillers demonstrate excellent dispersion within the polymeric matrix, as confirmed by the EDX results.

**4.2.3. Thermal properties.** The fabrication of polymer products with high thermal stability is one of the main objectives in the manufacturing of polymer materials, which is why the addition of fillers to the polymeric matrix is known to improve their thermal stability and alloy, these materials to be used in different application.[63] To study the thermal stability and degradation behavior of the composite materials, and to confirm the presence of the expected magnetic particle content in the HDPE matrix, thermogravimetric tests were carried out. Fig. 10 shows the TGA/DTG test results obtained from neat HDPE, NF-nano/HDPE and NF-micro/HDPE composite materials. Table S1† provides the corresponding *T* max and *T* onset values for both neat HDPE and composite materials, which were determined from the TGA analysis curves. There was a marginal increase in the onset temperature of HDPE by introducing the ferrite particles into it to form the composite. Further, samples with small particle size had higher onset temperature. TGA analyses reveal that neat HDPE and the composite materials are thermally stable up to 420 °C although a small weight loss of 5% was reported in this range which is most probably owing to the loss of water molecules entrapped in the HDPE polymer and composite materials as well as the decomposition polymer matrix.[64] The second weight loss, ranging from 420 °C to 488 °C only a single stage was observed, which corresponded to the entire weight loss, which is attributed to the full degradation of the polymeric matrix. In this part, the composite materials were lost only 59% of their weight, which indicated the presence of magnetic particles that were not degradable at this temperature.[65] The figure shows a small hump between 500 and 550 °C for the NF-nano/HDPE composite. This is attributed to the synthesis technique used for producing the magnetic nanoparticle surface. These residues decompose at higher temperature, causing the observed hump. In contrast, NF-micro particles synthesized *via* solid-state reaction methods do not involve surfactants, thereby avoiding this issue.[66–68] Additionally, nanoparticles have a significantly higher surface area to volume ratio compared to microparticles. This increased surface area can enhance the catalytic effect, promoting further decomposition of the polymer matrix at higher temperatures, which contributes to the observed hump.[66–68] The smaller size and higher surface energy of nanoparticles can lead to different interactions with the HDPE matrix, potentially causing minor phase transitions or reactions at elevated temperatures. These interactions are less significant in microparticles due to their large size and lower surface energy.[66–68]

Differential scanning calorimetry is used in this study to evaluate the effect of magnetic particles on the polymeric matrix HDPE. The DSC curve of neat HDPE and composite materials are shown in Fig. 11, while corresponding values are detailed in Table S2.† The result shows that NF-nano/HDPE and NF-micro/HDPE crystalline Fig. 11a, and melting peaks Fig. 11b, similar to those of pure HDPE. This phenomena indicate that the original crystal structure of the hosting matrix remains unchanged in spite of the incorporation of magnetic particles.[69] However, a significant finding was the increase in the crystalline temperature ($T_c$) for the HDPE based NF-nano and NF-micro particles. This was evident from the exothermic peak observed during the cooling phase of the DSC graph in Fig. 11. Specifically, $T_c$ values were recorded at 120.63 °C and 118.92 °C for NF-nano/HDPE and NF-micro/HDPE respectively. This result indicates that the existence of magnetic particles has initiated the large crystallites formation of HDPE at higher temperatures as compared to neat HDPE. Furthermore, the formation of the melting peak of all composite samples obtained by the endotherm during the heating portion of DSC thermogram. The addition of magnetic particles into HDPE matrix has retarded the peak melting temperature ($T_m$) to a higher temperature of 130.17 °C and 129.75 °C for NF-nano/HDPE and NF-micro/HDPE respectively as compared to its incidence at lower temperature 129.02 °C for neat HDPE, which made the composites materials more thermally stable.[70] The crystallinity $\chi_c$ of neat HDPE, NF-nano/HDPE and NF-micro/HDPE was determined using the following equation:

$$\chi_c = \frac{\Delta H_{exp}}{\Delta H W_f} \times 100\% \quad (6)$$

where $\Delta H_{exp}$ is the experimental melting enthalpy, $\Delta H$ is the enthalpy of melting of 100% crystalline neat HDPE which is

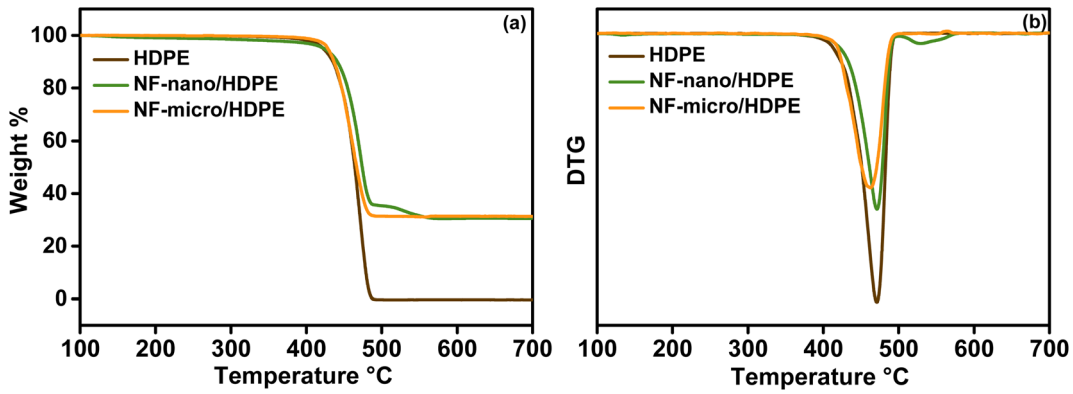


Fig. 10 (a) TGA and (b) DTG curves of pure HDPE, NF-micro/HDPE and NF-nano/HDPE composites.

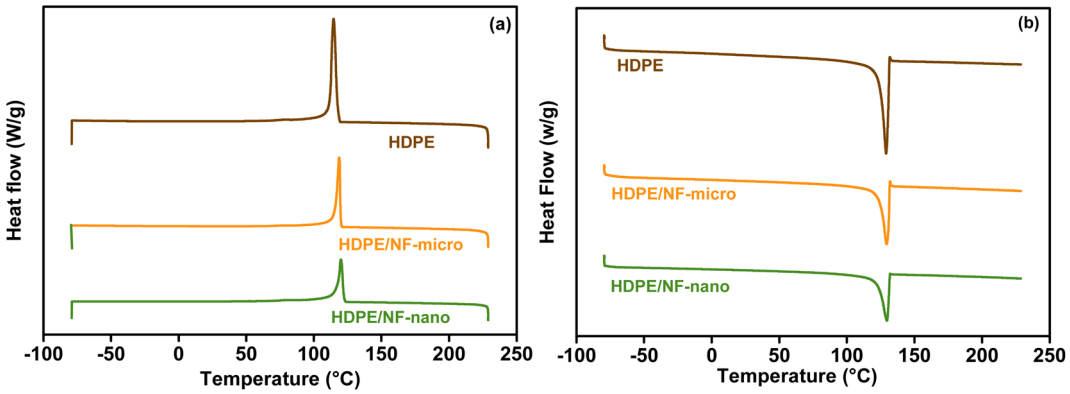


Fig. 11 DSC curve of composite materials and neat HDPE. (a) The heating curve and (b) the cooling curve.

292.6 j $g^{-1}$,[71] and $W_f$ is the weight fraction of HDPE.[72] From the result, a deceasing trend of $\chi_c$ is observed with the incorporation of $NiFe_2O_4$ nano and micro particles in HDPE matrix. This is attributed to the fact that the magnetic particles are able to disturb the continuity of the HDPE chains and thus introduce more grain boundaries and defects in the hosting matrix.[69]

**4.2.4. Mechanical properties.** The integration of magnetic composites based on polymer matrices into electromagnetic applications requires not only excellent magnetic properties but also superior mechanical properties. To investigate the mechanical properties of the produced HDPE based NF-nano or NF-micro particles, extensive tensile testing has been conducted, with detailed results depicted in Fig. 12a–c. These examinations reveal that the mechanical properties of polymer composites are significantly influenced by the incorporation of particles, with the effect being particularly dependent on the size of these fillers. It is clear from Fig. 12a the addition of both nanoparticles and microparticles strongly enhances the stiffness of the composite. This enhancement results from the particles limiting the polymer chains' mobility, which stiffens the material and improves its elastic response to applied stress. Specifically, compared to microparticles, nanoparticles have a greater surface area to volume ratio, which significantly restricts the mobility of the polymer chain and causes a more noticeable increase in Young's modulus.[73,74]

Regarding tensile strength (Fig. 12b), the improvement observed with the addition of filler particles is mainly due to the enhanced load transfer between the polymer matrix and the

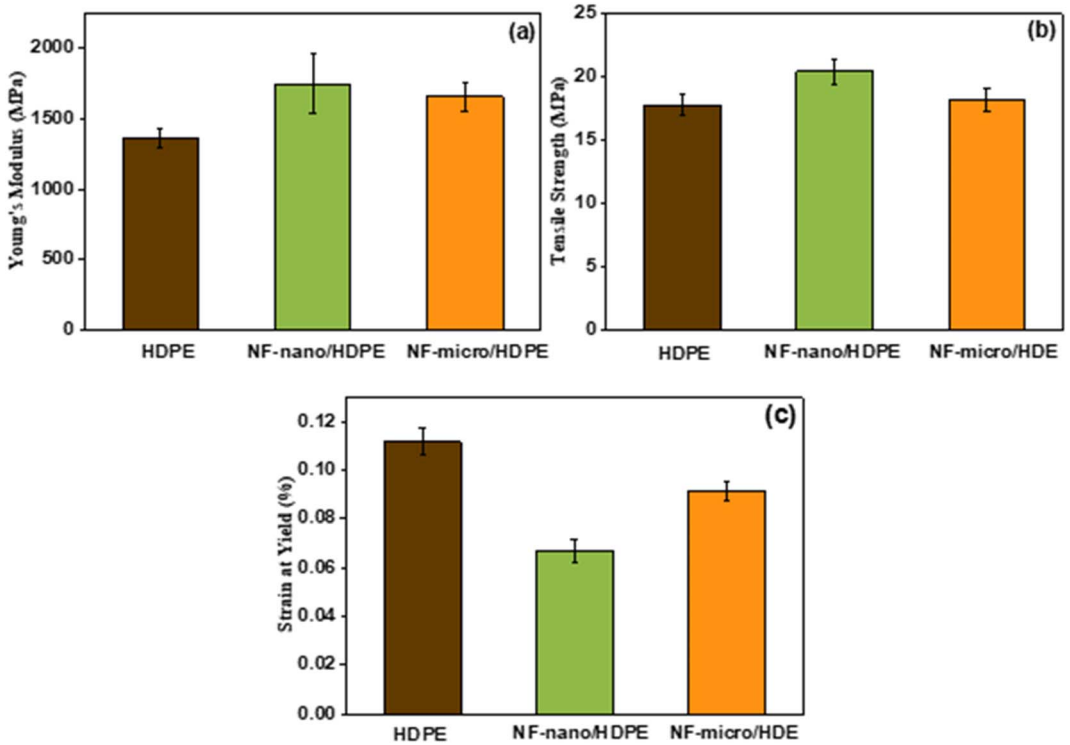


Fig. 12 Tensile test of neat HDPE and the elaborated composite materials.

filler. Due to their small size and large surface area of the nanoparticles, their interaction with the polymer matrix is further improved. This improved adhesion promotes a more efficient load distribution throughout the composite, resulting in considerably higher strength than the microparticles. The apparent difference in performance between nanofillers and microfillers emphasizes the important role of surfaces in promoting stronger interactions between polymers and fillers, leading to better mechanical properties.[75,76]

Moreover, the incorporation of filler particles affects the composite's ductility, evident from the decrease in strain at yield (Fig. 12c). This reduction indicates that the plastic deformability of the material is reduced, while the brittleness is increased due to the addition of fillers. In particular, due to the large surface area of the nanoparticles, they interact more effectively with the polymer matrix. This improved interaction significantly reduces the plastic deformability of the composites by facilitating efficient load transfer and restricting the mobility of the polymer chains.[77]

**4.2.5. Magnetic properties.** Magnetic hysteresis loops for magnetic composite material samples are plotted in Fig. 13. The result shows the magnetic behavior of NF-micro/HDPE and NF-nano/HDPE composite materials when exposed to an external magnetic field at room temperature. The highest saturation magnetizations value was obtained for the NF-micro/HDPE and NF-nano/HDPE samples is 22.13 emu $g^{-1}$ and 4.5 emu $g^{-1}$ respectively, reveal that magnetic particles are well distributed and dispersed within the polymer matrix Additionally, the maximum magnetization value is directly proportional to the amount of magnetic particles present in the polymer matrix.[78] If we compare between magnetic properties of nano/micro particles presented in Fig. 7 and magnetic properties of composite materials, we found that remananent magnetization ($M_r$) increases when the magnetic particles are incorporated in polymer matrix and also reveal small change in terms of the coercive field ($H_c$). These results indicate that there is a change in the magnetic properties when the particles are included in the composite.[79] The value of the coercive field ($H_c$), showed in Table 3, is slightly different, reaching a value of 0.04 Koe and 0.02 Koe for NF-micro/HDPE and NF-nano/HDPE respectively, which show that booth composites materials have soft magnetic behavior and that they require a low resistance to demagnetization, so it doesn't require a strong opposing magnetic field to demagnetize.[80] Remnant ratio of NF-micro/HDPE and NF-nano/HDPE have a value of 0.2 and 0.1 respectively which is a value significantly below 1, which demonstrates that the materials exhibit weak ferromagnetic behavior. The reduction in magnetization observed in NF-micro/HDPE and NF-nano/HDPE composites is directly associated with the quantity of magnetic particles present in the composite materials.

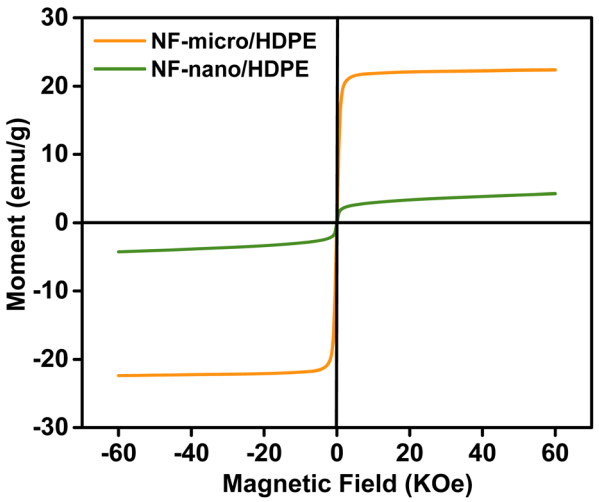


Fig. 13 Hysteresis loops of magnetic composite materials.

Table 3 Summary overview of magnetic parameters of composites materials

| Sample | $M_s$ (emu $g^{-1}$) | $M_r$ (emu $g^{-1}$) | $H_c$ (Koe) | $R$ |
|---|---|---|---|---|
| NF-micro/HDPE | 22.138 | 5.30 | 0.04 | 0.20 |
| NF-nano/HDPE | 4.50 | 0.5 | 0.03 | 0.1 |

## 5. Conclusion

The study show a new and coast effective technique, to produce a lightweight, high performance polymer magnetic composite materials based on high-density polyethylene as matrix for NF-nano and NF-micro particles fillers, using extrusion molding. It was found that the magnetic properties of magnetic particles are significantly impacted with the synthesis process. A good distribution of magnetic particles within the HDPE matrix was well demonstrated with the scanning electron microscopy (SEM). The mechanical properties of the composite materials are significantly affected by the presence of magnetic particles, influencing both flexibility are rigidity. A comparative analysis shows that, unlike NF-micro particles, NF-nano particles exhibit a more integrate more thoroughly into the polymer matrix, because of their large surface area, which lead to significantly reduces the plastic deformation of the composites due to the efficient transfer of loads and the associated mobility limitations of the polymer chains. The Vibrating Sample Magnetometer (VSM) results for the composite materials reveal that a uniform distribution of particles within the HDPE matrix alters the magnetic properties. The result also highlight the soft magnetic behavior of the composites and their low susceptibility to demagnetization. Overall, the developed polymers magnetic composite materials have offer a great properties, suggesting a promising future in several application (automotive, aeronautic, electromagnetic devises, *etc.*). Further research on polymer magnetic composite materials in spanned for the future, with a focus on optimizing the weight percentage of magnetic particles to achieve an optimal balance between magnetic and mechanical properties.

## Data availability

The data that support the findings of this study are available from the corresponding author, Mounir El Achaby, upon reasonable request.

## Conflicts of interest

There are no conflicts to declare.

## Acknowledgements

This research receives support from the Moroccan Ministry of Higher Education, Scientific Research, and Innovation, along with funding from the OCP Foundation through the APRD research program.

## References

1 M. D. Hossain, M. A. Hossain and S. S. Sikder, Hysteresis loop properties of rare earth doped spinel ferrites: A review, *J. Magn. Magn. Mater.*, 2022, **564**(P1), 170095, DOI: 10.1016/j.jmmm.2022.170095.

2 J. L. Xie, M. Han, L. Chen, R. Kuang and L. Deng, Microwave-absorbing properties of NiCoZn spinel ferrites, *J. Magn. Magn. Mater.*, 2007, **314**(1), 37–42.

3 H. Shokrollahi, A review of the magnetic properties, synthesis methods and applications of maghemite, *J. Magn. Magn. Mater.*, 2017, **426**(November 2016), 74–81, DOI: 10.1016/j.jmmm.2016.11.033.

4 S. Talebniya, I. Sharifi, M. R. Saeri and A. Doostmohammadi, Study of Cation Distribution and Magnetic Properties of MFe2O4 (M = Fe, Co, Zn, Mn, and Cu) Nanoparticles, *J. Supercond. Novel Magn.*, 2022, **35**(3), 899–908, DOI: 10.1007/s10948-021-06129-w.

5 J. M. Li and A. Huan, Interface effects on magnetoresistance and magnetic-field-reduced Raman scattering in magnetite, *Phys. Rev. B: Condens. Matter Mater. Phys.*, 2000, **61**(10), 6876–6878.

6 J. Xue, H. Zhang, J. Zhao, X. Ou and Y. Ling, Characterization and microwave absorption of spinel MFe2O4 (M = Mg, Mn, Zn) nanoparticles prepared by a facile oxidation-precipitation process, *J. Magn. Magn. Mater.*, 2020, **514**(June), 167168, DOI: 10.1016/j.jmmm.2020.167168.

7 H. Guo, J. L. Durham, A. B. Brady, A. C. Marschilok, E. S. Takeuchi, K. J. Takeuchi, *et al.*, Essential Role of Spinel MgFe 2 O 4 Surfaces during Discharge, *J. Electrochem. Soc.*, 2020, **167**(9), 090506.

8 X. B. Xie, B. Wang, Y. Wang, C. Ni, X. Sun and W. Du, Spinel structured MFe2O4 (M = Fe, Co, Ni, Mn, Zn) and their composites for microwave absorption: A review, *Chem. Eng. J.*, 2022, **428**(January 2021), 131160, DOI: 10.1016/j.cej.2021.131160.

9 T. Tatarchuk, M. Bououdina, J. Judith Vijaya and L. John Kennedy, Spinel ferrite nanoparticles: Synthesis, crystal structure, properties, and perspective applications, *Springer Proc. Phys.*, 2017, **195**, 305–325.

10 J. M. Li, X. L. Zeng and Z. A. Xu, Partial cationic inversion-induced magnetic hardening of densely packed 23-nm-sized nanocrystallite-interacting nickel ferrite electrospun nanowires, *Appl. Phys. Lett.*, 2013, **103**(23), 19–24.

11 K. K. Kefeni, T. A. M. Msagati, T. T. Nkambule and B. B. Mamba, Spinel ferrite nanoparticles and nanocomposites for biomedical applications and their toxicity, *Mater. Sci. Eng., C*, 2020, **107**, 110314, DOI: 10.1016/j.msec.2019.110314.

12 A. Makofane, P. J. Maake, M. M. Mathipa, N. Matinise, F. R. Cummings, D. E. Motaung, *et al.*, Green synthesis of $NiFe_2O_4$ nanoparticles for the degradation of Methylene Blue, sulfisoxazole and bacterial strains, *Inorg. Chem. Commun.*, 2022, **139**(March), 109348, DOI: 10.1016/j.inoche.2022.109348.

13 G. Rana, P. Dhiman, A. Kumar, D. V. N. Vo, G. Sharma, S. Sharma, *et al.*, Recent advances on nickel nano-ferrite: A review on processing techniques, properties and diverse applications, *Chem. Eng. Res. Des.*, 2021, **175**, 182–208, DOI: 10.1016/j.cherd.2021.08.040.

14 D. Chen, D. Chen, X. Jiao, Y. Zhao and M. He, Hydrothermal synthesis and characterization of octahedral nickel ferrite particles, *Powder Technol.*, 2003, **133**(1–3), 247–250.

15 K. M. Reddy, L. Satyanarayana, S. V. Manorama and R. D. K. Misra, A comparative study of the gas sensing behavior of nanostructured nickel ferrite synthesized by hydrothermal and reverse micelle techniques, *Mater. Res. Bull.*, 2004, **39**(10), 1491–1498.

16 K. Nejati and R. Zabihi, Preparation and magnetic properties of nano Mn-Zn ferrite particles, *Chem. Cent.*, 2012, **43**(1), 37–41. Available from: http://journal.chemistrycentral.com/content/6/1/23.

17 A. Makofane, P. J. Maake, M. M. Mathipa, N. Matinise, F. R. Cummings, D. E. Motaung, *et al.*, Green synthesis of $NiFe_2O_4$ nanoparticles for the degradation of Methylene Blue, sulfisoxazole and bacterial strains, *Inorg. Chem. Commun.*, 2022, **139**(March), 109348.

18 D. H. Chen and X. R. He, Synthesis of nickel ferrite nanoparticles by sol-gel method, *Mater. Res. Bull.*, 2001, **36**(7–8), 1369–1377.

19 G. R. Kumar, K. V. Kumar and Y. C. Venudhar, Synthesis, Structural and Magnetic Properties of Copper Substituted Nickel Ferrites by Sol-Gel Method, *Mater. Sci. Appl.*, 2012, **03**(02), 87–91.

20 R. Sen, P. Jain, R. Patidar, S. Srivastava, R. S. Rana and N. Gupta, Synthesis and Characterization of Nickel Ferrite ($NiFe_2O_4$) Nanoparticles Prepared by Sol- Gel Method, *Mater. Today: Proc.*, 2015, **2**(4–5), 3750–3757, DOI: 10.1016/j.matpr.2015.07.165.

21 M. A. S. Amulya, H. P. Nagaswarupa, M. R. A. Kumar, C. R. Ravikumar, S. C. Prashantha and K. B. Kusuma, Sonochemical synthesis of $NiFe_2O_4$ nanoparticles: Characterization and their photocatalytic and electrochemical applications, *Appl. Surf. Sci. Adv.*, 2020, **1**(June), 100023, DOI: 10.1016/j.apsadv.2020.100023.

22 K. V. P. M. Shafi, Y. Koltypin, A. Gedanken, R. Prozorov, J. Balogh, J. Lendvai, *et al.*, Sonochemical preparation of nanosized amorphous $NiFe_2O_4$ particles, *J. Phys. Chem. B*, 1997, **101**(33), 6409–6414.

23 S. S. Jadhav, S. E. Shirsath, B. G. Toksha, S. M. Patange, D. R. Shengule and K. M. Jadhav, Structural and electric properties of zinc substituted $NiFe_2O_4$ nanoparticles

prepared by co-precipitation method, *Phys. B*, 2010, **405**(12), 2610–2614, DOI: 10.1016/j.physb.2010.03.008.

24 S. Kazi, S. Inamdar, Y. sarnikar, D. Kamble and R. Tigote, Simple Co-precipitation synthesis and characterization of magnetic spinel $NiFe_2O_4$ nanoparticles, *Mater. Today: Proc.*, 2022, **73**(3), 448–454.

25 T. Jahanbin, M. Hashim and K. Amin Mantori, Comparative studies on the structure and electromagnetic properties of Ni-Zn ferrites prepared via co-precipitation and conventional ceramic processing routes, *J. Magn. Magn. Mater.*, 2010, **322**(18), 2684–2689, DOI: 10.1016/j.jmmm.2010.04.008.

26 P. Thakur, S. Taneja, D. Chahar, B. Ravelo and A. Thakur, Recent advances on synthesis, characterization and high frequency applications of Ni-Zn ferrite nanoparticles, *J. Magn. Magn. Mater.*, 2021, **530**(October 2020), 167925, DOI: 10.1016/j.jmmm.2021.167925.

27 S. Kumar, F. Ahmed, N. M. Shaalan, N. Arshi, S. Dalela and K. H. Chae, *Properties of $NiFe_2O_4$ Nanoparticles as Electrode Materials for Supercapacitor Applications*, 2023.

28 H. Lu, Y. Dong, X. Liu, Z. Liu, Y. Ma, Y. Wu, *et al.*, Enhanced magnetic properties of FeSiAl soft magnetic composites prepared by utilizing phosphate: PSA as insulating layer, *J. Mater. Sci.: Mater. Electron.*, 2022, **33**(13), 10131–10141.

29 R.-M. Wang, S.-R. Zheng and Y.-P. Zheng, Introduction to polymer matrix composites, *Polymer Matrix Composites and Technology*, 2011, pp. 1–548.

30 F. Z. Semlali, A. Ait Benhamou, K. El Bourakadi, A. E. K. Qaiss, R. Bouhfid, J. Jacquemin, *et al.*, Thermo-compression process-mediated in-situ cellulose microfibers phosphorylation enables high performant cellulosic paper packaging, *Chem. Eng. J.*, 2023, **473**(March), 145268.

31 S. Kalia, S. Kango, A. Kumar, Y. Haldorai, B. Kumari and R. Kumar, Magnetic polymer nanocomposites for environmental and biomedical applications, *Colloid Polym. Sci.*, 2014, **292**(9), 2025–2052.

32 J. L. Wilson, P. Poddar, N. A. Frey, H. Srikanth, K. Mohomed, J. P. Harmon, *et al.*, Synthesis and magnetic properties of polymer nanocomposites with embedded iron nanoparticles, *J. Appl. Phys.*, 2004, **95**(3), 1439–1443.

33 I. Kong, S. H. Ahmad, M. H. Abdullah and A. N. Yusoff, The effect of temperature on magnetic behavior of magnetite nanoparticles and its nanocomposites, *AIP Conf. Proc.*, 2009, **1136**, 830–834.

34 Y. C. Chung, J. W. Choi, M. W. Choi and B. C. Chun, Characterization of flexibly linked shape memory polyurethane composite with magnetic property, *J. Thermoplast. Compos. Mater.*, 2012, **25**(3), 283–303.

35 R. T. Araujo, G. R. Ferreira, T. Segura, F. G. Souza and F. Machado, An experimental study on the synthesis of poly(vinyl pivalate)-based magnetic nanocomposites through suspension polymerization process, *Eur. Polym. J.*, 2015, **68**, 441–459, DOI: 10.1016/j.eurpolymj.2015.05.015.

36 R. Hsissou, R. Seghiri, Z. Benzekri, M. Hilali, M. Rafik and A. Elharfi, Polymer composite materials: A comprehensive review, *Compos. Struct.*, 2021, **262**, 113640.

37 T. Tatarchuk, M. Bououdina, W. Macyk, O. Shyichuk, N. Paliychuk, I. Yaremiy, *et al.*, Structural, Optical, and Magnetic Properties of Zn-Doped CoFe2O4 Nanoparticles, *Nanoscale Res. Lett.*, 2017, **12**(141), 1–11.

38 J. Singh, A. Roychoudhury, M. Srivastava, V. Chaudhary, R. Prasanna, D. W. Lee, *et al.*, Highly efficient bienzyme functionalized biocompatible nanostructured nickel ferrite-chitosan nanocomposite platform for biomedical application, *J. Phys. Chem. C*, 2013, **117**(16), 8491–8502.

39 Z. Y. Yu, L. F. Chen and S. H. Yu, Growth of $NiFe_2O_4$ nanoparticles on carbon cloth for high performance flexible supercapacitors, *J. Mater. Chem. A*, 2014, **2**(28), 10889–10894.

40 L. Chauhan, A. K. Shukla and K. Sreenivas, Dielectric and magnetic properties of Nickel ferrite ceramics using crystalline powders derived from DL alanine fuel in sol-gel auto-combustion, *Ceram. Interfaces*, 2015, **41**(7), 8341–8351, DOI: 10.1016/j.ceramint.2015.03.014.

41 Y. Y. Liao, Y. W. Li, Z. G. Hu and J. H. Chu, Temperature dependent phonon Raman scattering of highly a-axis oriented CoFe 2O 4 inverse spinel ferromagnetic films grown by pulsed laser deposition, *Appl. Phys. Lett.*, 2012, **100**(7), DOI: 10.1063/1.3683520.

42 R. S. Yadav, I. Kuřitka, J. Vilcakova, J. Havlica, J. Masilko, L. Kalina, *et al.*, Structural, magnetic, dielectric, and electrical properties of $NiFe_2O_4$ spinel ferrite nanoparticles prepared by honey-mediated sol-gel combustion, *J. Phys. Chem. Solids*, 2017, **107**(February), 150–161.

43 M. H. Habibi and H. J. Parhizkar, FTIR and UV-vis diffuse reflectance spectroscopy studies of the wet chemical (WC) route synthesized nano-structure CoFe2O4 from CoCl2 and FeCl3, *Spectrochim. Acta, Part A*, 2014, **127**, 102–106, DOI: 10.1016/j.saa.2014.02.090.

44 Y. H. Utari and K. Dasi, Comparison of $Ni_{0.6}Co_{0.4}Fe_2O_4$ and $NiFe_2O_4$ Nanoparticles for Magnetic Characteristics, Synthesized Using Co-Precipitation Method, *Int. J. Nano Res.*, 2022, **12**(1), 61–66.

45 M. Sundararajan, M. Sukumar, C. S. Dash, A. Sutha, S. Suresh, M. Ubaidullah, *et al.*, A comparative study on $NiFe_2O_4$ and $ZnFe_2O_4$ spinel nanoparticles: Structural, surface chemistry, optical, morphology and magnetic studies, *Phys. B*, 2022, **644**(April), 414232, DOI: 10.1016/j.physb.2022.414232.

46 S. Ez-Zahraoui, F. Z. Semlali Aouragh Hassani, R. Bouhfid, A. E. K. Qaiss and M. El Achaby, Strengthening effect of phosphate sludge by-product and styrene-butadiene rubber on the properties of high-density polyethylene composites, *Composites, Part A*, 2023, **166**(August 2022), 107378.

47 P. N. Medeiros, Y. F. Gomes, M. R. D. Bomio, I. M. G. Santos, M. R. S. Silva, C. A. Paskocimas, *et al.*, Influence of variables on the synthesis of CoFe2O4 pigment by the complex polymerization method, *J. Adv. Ceram.*, 2015, **4**(2), 135–141.

48 R. Masrour, H. El Moussaoui, E. Salmani, O. Mounkachi, H. Ez-Zahraouy, M. Hamedoun, *et al.*, Synthesis and magnetic properties of bulk ferrites spinels Ni 0.5 Zn 0.5 Fe 2 O 4 : Experimental an *Ab initio* study, *J. Supercond. Novel Magn.*, 2014, **27**(1), 177–181.

49 S. Karmakar, *Magnetic and Optical Studies of $NiFe_2O_4$ Micro- and Nanoparticles*, 2019.
50 F. El Bachraoui, Z. Chchiyai, Y. Tamraoui, H. El Moussaoui, J. Alami and B. Manoun, Optical and magnetic properties of perovskite materials: Ba0.3La0.7Ti0.3Fe0.7O3 and Ba0.1La0.9Ti0.1Fe0.9O3, *J. Rare Earths*, 2022, **40**(4), 652–659, DOI: 10.1016/j.jre.2021.05.008.
51 D. Bouokkeze, J. Massoudi, W. Hzez, M. Smari, A. Bougoffa, K. Khirouni, *et al.*, Investigation of the structural, optical, elastic and electrical properties of spinel LiZn2Fe3O8 nanoparticles annealed at two distinct temperatures, *RSC Adv.*, 2019, **9**(70), 40940–40955.
52 P. Chitra, E. R. Kumar, T. Pushpagiri and A. Steephen, Size and Phase Purity–Dependent Microstructural and Magnetic Properties of Spinel Ferrite Nanoparticles, *J. Supercond. Novel Magn.*, 2021, **34**(4), 1239–1244.
53 Z. Zhang, Y. Liu, G. Yao, G. Zu, X. Zhang and J. Ma, Solid-state reaction synthesis of $NiFe_2O_4$ nanoparticles by optimizing the synthetic conditions, *Phys. E*, 2012, **45**, 122–129, DOI: 10.1016/j.physe.2012.07.019.
54 K. Maaz, S. Karim, A. Mumtaz, S. K. Hasanain, J. Liu and J. L. Duan, Synthesis and magnetic characterization of nickel ferrite nanoparticles prepared by co-precipitation route, *J. Magn. Magn. Mater.*, 2009, **321**(12), 1838–1842.
55 D. E. Cvejić, G. Ivković Ivandekić, B. Bajac, P. Postolache, L. Mitoseriu, *et al.*, The effect of annealing on microstructure and cation distribution of $NiFe_2O_4$, *J. Alloys Compd.*, 2015, **649**, 1231–1238.
56 Z. Zi, Y. Sun, X. Zhu, Z. Yang, J. Dai and W. Song, Synthesis and magnetic properties of CoFe2O4 ferrite nanoparticles, *J. Magn. Magn. Mater.*, 2009, **321**(9), 1251–1255.
57 H. Li, H. Z. Wu and G. X. Xiao, Effects of synthetic conditions on particle size and magnetic properties of $NiFe_2O_4$, *Powder Technol.*, 2010, **198**(1), 157–166, DOI: 10.1016/j.powtec.2009.11.005.
58 R. S. Kamal, M. M. Shaban, G. Raju and R. K. Farag, High-Density Polyethylene Waste (HDPE)-Waste-Modified Lube Oil Nanocomposites as Pour Point Depressants, *ACS Omega*, 2021, **6**(47), 31926–31934.
59 M. R. Nivitha, E. Prasad and J. M. Krishnan, Ageing in modified bitumen using FTIR spectroscopy, *Int. J. Pavement Eng.*, 2016, **17**(7), 565–577.
60 D. J. da Silva and H. Wiebeck, Predicting LDPE/HDPE blend composition by CARS-PLS regression and confocal Raman spectroscopy, *Polimeros*, 2019, **29**(1), 1–7.
61 G. Thejas Urs, R. V. Hurkadli, R. V. Basavaraj, M. Niranjana, A. Manjunath and R. Somashekar, Study of optical and conducting properties of FeCl3 doped PVA polymers, *Prog. Cryst. Growth Charact. Mater.*, 2014, **60**(3–4), 87–93, DOI: 10.1016/j.pcrysgrow.2014.09.003.
62 O. O. Daramola, O. G. Agbabiaka, I. O. Oladele and D. M. Marindoti, Influence of Silica Sand Particles on the Tensile Properties and Water Absorption Behaviour of high density polyethylene matrix composites, *Int. J. Eng.*, 2016, 195–201.
63 K. H. Su, C. Y. Su, W. L. Shih and F. T. Lee, Improvement of the Thermal Conductivity and Mechanical Properties of 3D-Printed Polyurethane Composites by Incorporating Hydroxylated Boron Nitride Functional Fillers, *Materials*, 2023, **16**(1), 356.
64 G. D. Prasanna, H. S. Jayanna, A. R. Lamani and S. Dash, Polyaniline/CoFe2O4 nanocomposites: A novel synthesis, characterization and magnetic properties, *Synth. Met.*, 2011, **161**(21–22), 2306–2311, DOI: 10.1016/j.synthmet.2011.08.039.
65 M. Zighed and B. Benotmane, Performance of high-density polyethylene–starch–linen fiber biocomposite, *Iran. Polym. J.*, 2022, **31**(6), 751–760, DOI: 10.1007/s13726-022-01035-x.
66 L. T. Lu, N. T. Dung, L. D. Tung, C. T. Thanh, O. K. Quy, N. V. Chuc, *et al.*, Synthesis of magnetic cobalt ferrite nanoparticles with controlled morphology, monodispersity and composition: The influence of solvent, surfactant, reductant and synthetic conditions, *Nanoscale*, 2015, **7**(46), 19596–19610.
67 M. S. Rao, C. S. Rao and A. S. Kumari, Synthesis, stability, and emission analysis of magnetite nanoparticle-based biofuels, *J. Eng. Appl. Sci.*, 2022, **69**(1), 1–38, DOI: 10.1186/s44147-022-00127-y.
68 A. Schoth, A. D. Keith, K. Landfester and R. Muñoz-Espí, Silanization as a versatile functionalization method for the synthesis of polymer/magnetite hybrid nanoparticles with controlled structure, *RSC Adv.*, 2016, **6**(59), 53903–53911.
69 Q. He, T. Yuan, J. Zhu, Z. Luo, N. Haldolaarachchige, L. Sun, *et al.*, Magnetic high density polyethylene nanocomposites reinforced with in-situ synthesized Fe@FeO core-shell nanoparticles, *Polymer*, 2012, **53**(16), 3642–3652, DOI: 10.1016/j.polymer.2012.06.010.
70 D. Shahdan, M. H. Flaifel, S. H. Ahmad, R. S. Chen and J. A. Razak, Enhanced magnetic nanoparticles dispersion effect on the behaviour of ultrasonication-assisted compounding processing of PLA/LNR/NiZn nanocomposites, *J. Mater. Res. Technol.*, 2021, **15**, 5988–6000, DOI: 10.1016/j.jmrt.2021.11.046.
71 M. I. S. Aguiar, A. F. Sousa, G. Teixeira, A. P. M. Tavares, A. M. Ferreira and J. A. P. Coutinho, Enhancing plastic waste recycling: Evaluating the impact of additives on the enzymatic polymer degradation, *Catal. Today*, 2024, **429**(December 2023), 1–8.
72 D. Shahdan, S. Ahmad, R. S. Chen, A. Omar, F. D. Zailan and N. A. Abu Hassan, Mechanical performance, heat transfer and conduction of ultrasonication treated polyaniline bio-based blends, *Int. Commun. Heat Mass Transfer*, 2020, **117**, 104742.
73 S. Y. Fu, X. Q. Feng, B. Lauke and Y. W. Mai, Effects of particle size, particle/matrix interface adhesion and particle loading on mechanical properties of particulate-polymer composites, *Composites, Part B*, 2008, **39**(6), 933–961.
74 S. E. Zahraoui, F. Z. Semlali, M. Raji and F. Z. Nazih, Synergistic reinforcing effect of fly ash and powdered wood chips on the properties of polypropylene hybrid composites, *J. Mater. Sci.*, 2023, **59**, 1417–1432.
75 D. R. Paul and L. M. Robeson, Polymer nanotechnology: Nanocomposites, *Polymer*, 2008, **49**(15), 3187–3204.

76 S. Ez-Zahraoui, S. Sabir, S. Berchane, R. Bouhfid, A. E. K. Qaiss, F.-Z. Semlali Aouragh Hassani, *et al.*, Toughening effect of thermoplastic polyurethane elastomer on the properties of fly ash-reinforced polypropylene-based composites, *Polym. Compos.*, 2022, 1–12.

77 S. Kango, S. Kalia, A. Celli, J. Njuguna, Y. Habibi and R. Kumar, Surface modification of inorganic nanoparticles for development of organic-inorganic nanocomposites - A review, *Prog. Polym. Sci.*, 2013, **38**(8), 1232–1261.

78 P. Martins, Y. V. Kolen'Ko, J. Rivas and S. Lanceros-Mendez, Tailored Magnetic and Magnetoelectric Responses of Polymer-Based Composites, *ACS Appl. Mater. Interfaces*, 2015, **7**(27), 15017–15022.

79 P. S. Antonel, F. M. Berhó, G. Jorge and F. V. Molina, Magnetic composites of CoFe2O4 nanoparticles in a poly(aniline) matrix: Enhancement of remanence ratio and coercivity, *Synth. Met.*, 2015, **199**, 292–302, DOI: **10.1016/j.synthmet.2014.12.003**.

80 A. Mooti, C. M. Costa, A. Maceiras, N. Pereira, C. R. Tubio, J. L. Vilas, *et al.*, Magnetic and high-dielectric-constant nanoparticle polymer tri-composites for sensor applications, *J. Mater. Sci.*, 2020, **55**(34), 16234–16246, DOI: **10.1007/s10853-020-05165-6**.